# A micromechanical model for martensitic phase-transformations in shape-memory alloys based on energy-relaxation

**ARTICLE** *in* ZAMM JOURNAL OF APPLIED MATHEMATICS AND MECHANICS: ZEITSCHRIFT FÜR ANGEWANDTE MATHEMATIK UND MECHANIK · OCTOBER 2009

Impact Factor: 1.16 · DOI: 10.1002/zamm.200900244

ZAMM · Z. Angew. Math. Mech. **89**, No. 10, 792 – 809 (2009) / **DOI** 10.1002/zamm.200900244

# A micromechanical model for martensitic phase-transformations in shape-memory alloys based on energy-relaxation

**Thorsten Bartel**[1,*] **and Klaus Hackl**[2,**]

[1] Institute of Mechanics, Dortmund University of Technology, 44227 Dortmund, Germany
[2] Institute of Mechanics, University of Bochum, 44780 Bochum, Germany

Received 2 February 2009, revised 11 July 2009, accepted 23 July 2009
Published online 7 September 2009

**Key words** Martensitic phase transformations, shape-memory alloys, energy relaxation, quasi-convexification.

We develop a micromechanical model for single-crystalline materials undergoing diffusionless solid-to-solid phase transitions. It is based on the specification of laminated microstructures on the materials' microscale and hence is designed to approximate the rank-1-convex hull of the underlying energy-density for the phase-mixture. In order to capture the hysteretic behavior of such materials like shape-memory-alloys we also account for dissipation by means of evolution equations for the inelastic internal variables. In this context, we derive different evolution-laws from inelastic potentials via least-action principles. Several material-point computations emphasize the characteristics of the presented model.



## 1 Introduction

Material models for solid-to-solid phase-transitions have been frequently developed during the last decade, almost all of them for the purpose of simulating the material behavior of shape-memory alloys (SMA). Even among the family of micromechanical models the variety of different concepts is wide. In this regard, we follow the concept of energy-relaxation which is closely related to the so-called direct methods of the calculus of variations and quasiconvexification, respectively (see for example [9, 32, 35]).

As outlined in [4], our purpose is to adapt theories presented in [3, 6] and apply them to martensitic phase-transformations especially within SMAs taking into account the possibility for the parent phase austenite to be transformed into several crystallographic variants of martensite depending on the specific material (CuAlNi or NiTi, for instance). This feature of the model outlines the main difference to phenomenological models as stated in [1, 23, 39], where just one general martensite-phase is considered. Furthermore, it is even possible to gain understanding regarding processes taking place on the microscale of the material due to the evolution of the underlying microstructure.

An exact quasiconvex hull for the geometrically linear case has been derived in [29] and [45] in the context of a double-well and a three-well potential, respectively. As shown in [10] and [11], it is possible to derive an exact quasiconvex hull for so-called nematic elastomers even for large deformations. The scope of our work is to derive an approximation of the quasiconvex envelope of a multi-well potential and hence shares the philosophy of models presented in [7, 13–15]. To enhance such approaches with dissipative aspects we make use of variational principles for inelastic solids as pointed out in [33, 34, 36, 37] which leads to the derivation of evolution equations from a dissipation potential. In this context, we derive different kinds of evolution laws, namely of von Mises-, Tresca-, and Perzyna-type, underlining the multifunctional character of the overall concept. Micromechanical models related to that presented in this work have been introduced in [13, 21, 22] for single crystals and in [17, 18] for polycrystals. A phenomenological model for polycristalline shape memory alloys is also presented in [30]. In the context of thin films, the model provided in [42] also takes into account multiple variants of martensite. Comparisons with experimental results can be found in [19, 20].

Since the applied method can be regarded as a homogenization procedure due to the fact that we do not take into account the lath-width of laminates present within a representative volume element (RVE) surface energies at the phase boundaries are neglected. In order to capture these effects as well one would have to solve a full boundary value problem on the level of the RVE as stated in [8, 25, 26].

* Corresponding author E-mail: thorsten.bartel@udo.edu, Phone: +49 231 755 2668, Fax: +49 231 755 2688
** E-mail: klaus.hackl@rub.de, Phone: +49 234 32 26025, Fax: +49 234 32 14154

## 2 Continuum-mechanical framework

### 2.1 Martensitic variants

According to [2] and as explained for instance in [5], the transformation from austenite to martensite can be described by a homogeneous deformation of the crystallographic lattice. Hence, it is possible to find symmetric matrices $\mathbf{U}_I^t$ describing such deformations from the austenitic to the lattice of the $I$-th martensitic variant. These matrices are often referred to as Bain matrices or transformation matrices and can be identified as right stretch-tensors in the continuum-mechanical context. Depending on the kind of transformation, e.g. cubic to monoclinic, there exist several possible variants of martensite, whose number will be denoted by $NV$ (Number of Variants) from now on. The specific value of $NV$ depends of course on the type of crystallographic symmetry.

In this work, we will restrict ourselves to the consideration of small deformations. Thus, the Biot-strain

$$\boldsymbol{\varepsilon}_I^t := \mathbf{U}_I^t - \mathbf{I} \tag{1}$$

is used as physically well suited measure, where $\mathbf{I}$ denotes the identity matrix. Values for those transformation-strains are provided in Appendix A.

### 2.2 Phase energies

The micromechanical model is based on quadratic energy densities

$$\psi_I = \frac{1}{2}\,\boldsymbol{\varepsilon}_I^e : \mathbf{C}_I : \boldsymbol{\varepsilon}_I^e + \mathcal{C}_I \tag{2}$$

for each phase $I$ of the material, where $\boldsymbol{\varepsilon}_I^e$ represents the elastic part of the deformation, namely

$$\boldsymbol{\varepsilon}_I^e = \boldsymbol{\varepsilon} - \boldsymbol{\varepsilon}_I^t \quad , \tag{3}$$

and $\mathbf{C}_I$ represents the fourth-order material tensor for each phase. Moreover, $\mathcal{C}_I$ denotes temperature-dependent chemical energies. Taking into account that transformation-strains for the parent phase austenite $\boldsymbol{\varepsilon}_A^t$ are zero and using (3) leads us to

$$\psi_A\left(\boldsymbol{\varepsilon}\right) = \frac{1}{2}\,\boldsymbol{\varepsilon} : \mathbf{C}_A : \boldsymbol{\varepsilon} + \mathcal{C}_A \tag{4}$$

$$\psi_{M,I}\left(\boldsymbol{\varepsilon}\right) = \frac{1}{2}\,\left(\boldsymbol{\varepsilon} - \boldsymbol{\varepsilon}_I^t\right) : \mathbf{C}_M : \left(\boldsymbol{\varepsilon} - \boldsymbol{\varepsilon}_I^t\right) + \mathcal{C}_M \quad , I = 1 \ldots NV \tag{5}$$

as austenitic and martensitic phase energy-densities where we now assume $\mathcal{C}_I = \mathcal{C}_M \,\forall I = 1 \ldots NV$. To follow the concept of energy-relaxation an averaged energy-density within the RVE is required. The first step towards the determination of the desired quasiconvex hull of such functionals is to allocate different states of total strain, namely $\boldsymbol{\varepsilon}_A$ and $\boldsymbol{\varepsilon}_I, I = 1 \ldots NV$, to each phase, which is discussed in [38] in detail. Hence,

$$\psi = \theta_A\,\psi_A\left(\boldsymbol{\varepsilon}_A\right) + \sum_{I=1}^{NV} \theta_I\,\psi_{M,I}\left(\boldsymbol{\varepsilon}_I\right) \tag{6}$$

denotes the averaged energy-density of the RVE, where the volume fractions of each martensite-variant $\theta_I$ along with

$$\theta_A := (1 - \theta_M) \tag{7}$$

$$\theta_M := \sum_{I=1}^{NV} \theta_I \tag{8}$$

as overall portions of austenite/martensite have been introduced. In this context, the following restrictions

$$r_I := -\theta_I \leq 0 \quad , I = 1 \ldots NV \quad ; \qquad \bar{r} := \theta_M - 1 \leq 0 \tag{9}$$

need to be fulfilled throughout the model, which will be discussed in detail in one of the following sections.

## 3 Microstructure and relaxation

In contrast to purely thermodynamical theories of phase-mixtures (e.g. change of aggregate states) the formation of new phases within solid materials is subjected to the creation of meaningful deformation patterns in terms of compatibility of strains. The application of Gibbs-type laws for phase-mixtures, which incidentally coincides with pure convexification of a corresponding multi-well potential, see [9, 43], cannot fulfill any compatibility among deformations within patterns of different solid phases. Since our aim is to directly incorporate informations about the microstructure in our model we make use of a more sophisticated method here although convexification may yield surprisingly good results as shown in [13, 14].

In this work we will apply the concept of relaxation in terms of finding the so-called quasiconvex envelope of the multi-well potential corresponding to the various variants of the material. The quasiconvex envelope guarantees on the one hand that a solution of the energy minimization problem exists from the mathematical point of view. Consequently, numerical approximations are mesh-independent. On the other hand physical plausibility is achieved by introducing well-defined microstructures involving only physically well-understood parameters.

The quasiconvex envelope of an underlying functional (in our case (6)),

$$Q\psi\left(\boldsymbol{\varepsilon}\right) = \min\left\{ \int\limits_{[0,1]^d} \psi\left(\boldsymbol{\varepsilon} + \nabla_S \boldsymbol{\varphi}\right)\, dV; \boldsymbol{\varphi} \right\} \quad , \tag{10}$$

can be obtained by the superposition of a periodic perturbation field $\boldsymbol{\varphi} \in W^{1,\infty}_{\mathrm{per}}([0,1]^d, \mathbb{R}^d)$ to the homogeneous displacements corresponding to the macroscopic strains (see for example [9, 43]) and a subsequent minimization with respect to $\boldsymbol{\varphi}$, where $d$ denotes the spatial dimension of the problem. Hence, the spatially varying microscopic strains are given by $\boldsymbol{\varepsilon} + \nabla_S \boldsymbol{\varphi}$, where $\nabla_S \boldsymbol{\varphi} := 1/2\left(\nabla \boldsymbol{\varphi} + \boldsymbol{\varphi} \nabla\right)$. Since $\boldsymbol{\varphi}$ is designed to minimize an integral expression and can be any admissible function, the quasiconvex envelope can only be computed in rare cases. Thus, we will specify $\boldsymbol{\varphi}$ in the spirit of [5, 13, 24, 27, 28] via lamination yielding an upper bound to the quasiconvex hull.

In this sense, the displacement-field on the microscale $\mathbf{u} = \mathbf{u}^{\mathrm{hom}} + \mathbf{u}^{\mathrm{pert}}$ is decomposed into a homogeneous part $\mathbf{u}^{\mathrm{hom}} = \boldsymbol{\varepsilon} \cdot \mathbf{x}$ and a perturbation-field $\mathbf{u}^{\mathrm{pert}}$. Our ansatz for these perturbations is exemplarily depicted for $NV = 3$ and two dimensional space in Figs. 1 to 3 and will be discussed in detail now. Laminates of first order are introduced for the purpose of distinguishing austenite and martensite as well as second order laminates within the martensite-regimes to separate different variants. These laminates are aligned in directions $\mathbf{n}_A$ and $\mathbf{n}_M$, respectively. Accordingly, we consider roof-like perturbations depending on the projections $\xi := \mathbf{x} \cdot \mathbf{n}_A$ and $\zeta := \mathbf{x} \cdot \mathbf{n}_M$, where the amplitudes are specified as $\mathbf{u}_A$ and $\mathbf{u}_I$, $I = 1 \ldots NV - 1$ representing additional internal variables. These perturbations can be mathematically expressed by

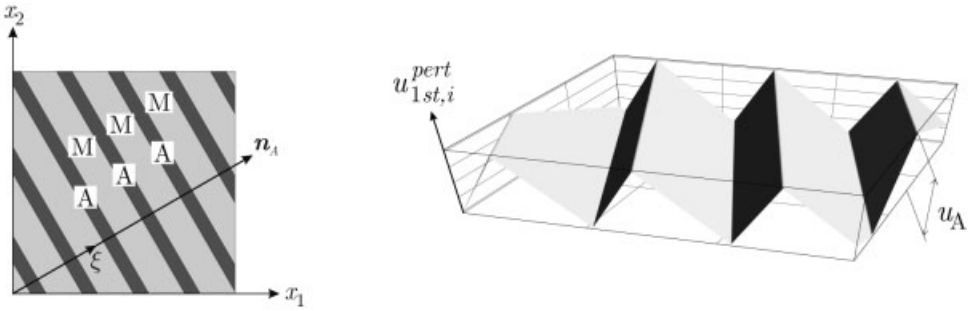


**Fig. 1** 'Roof-like' perturbations are superimposed to each component $i$ of local displacements along the direction of 1st order laminates $\mathbf{n}_A$ with a maximum amplitude $\mathbf{u}_A$ leading to a 'symmetrized' rank-one compatibility of strains.

$$\mathbf{u}^{\mathrm{pert}}_{1st} = \begin{cases} \mathbf{u}^{\mathrm{pert}}_A = \frac{1}{\theta_A}\, \mathbf{u}_A\, (\xi - i + 1) & \text{, if } i - 1 \leq \xi \leq i - 1 + \theta_A \\ \mathbf{u}^{\mathrm{pert}}_M = -\frac{1}{\theta_M}\, \mathbf{u}_A\, (\xi - i) & \text{, else} \end{cases} \tag{11}$$

and

$$\mathbf{u}^{\mathrm{pert}}_I = \mathbf{u}^{\mathrm{pert}}_M + \frac{1}{\theta_I}\left(\mathbf{u}_I - \mathbf{u}_{I-1}\right)\left(\zeta - \sum_{k=1}^{I-1}\{\theta_k\} - (j-1)\theta_M\right) + \mathbf{u}_{I-1} \tag{12}$$

 

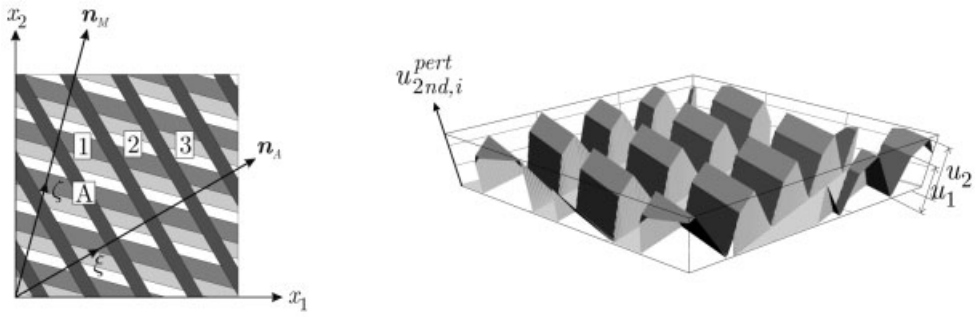


**Fig. 2** Additional perturbations are applied to the martensite-regimes in order to account for different crystallographic variants (here exemplarily depicted for $NV = 3$). This implies additional micromechanical variables $\mathbf{n}_M$ and $\mathbf{u}_I, I = 1 \ldots NV - 1$.

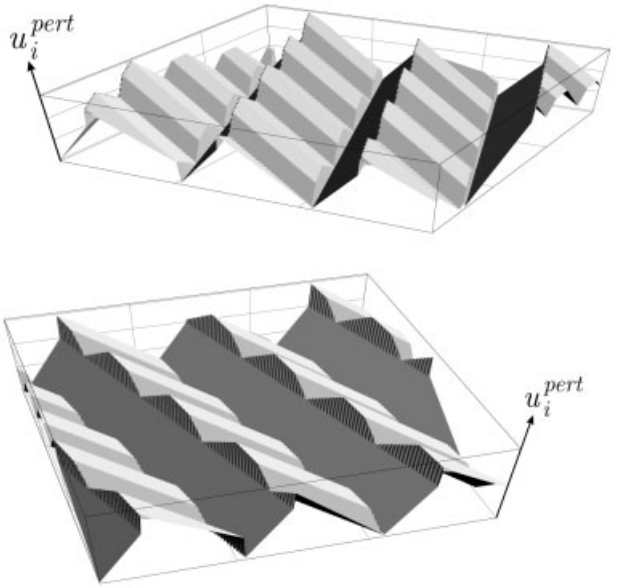


**Fig. 3** Total perturbations of local displacements in two different views for the sake of clarity. Obviously, displacements are not compatible. However, the mean values of resulting strains are equal to the macroscopic ones and moreover 'rank-one-connected' in a symmetrized form.

$$\mathbf{u}^{\text{pert}}_{2nd} = \begin{cases} \mathbf{u}^{\text{pert}}_1 & \text{, if } i-1+\theta_A \le \xi \le i \ \wedge\ j-1 \le \zeta \le j-1+\theta_1 \\ \mathbf{u}^{\text{pert}}_2 & \text{, if } i-1+\theta_A \le \xi \le i \ \wedge\ j-1+\theta_1 \le \zeta \le j-1+\theta_1+\theta_2 \\ \vdots & \\ 0 & \text{, else} \end{cases} \tag{13}$$

where $i = 1, 2, \ldots$ and $j = 1, 2, \ldots$ denote the current periodic pattern of 1st order and second order laminates, respectively. This results in an overall perturbation-field $\mathbf{u}^{\text{pert}} = \mathbf{u}^{\text{pert}}_{1st} + \mathbf{u}^{\text{pert}}_{2nd}$ which is shown in Fig. 3. In a straight forward way one obtains

$$\boldsymbol{\varepsilon}_A = \boldsymbol{\varepsilon} + \frac{1}{\theta_A}\, \mathbf{n}_A \otimes_S \mathbf{u}_A \tag{14}$$

$$\boldsymbol{\varepsilon}_I = \boldsymbol{\varepsilon} - \frac{1}{\theta_M}\, \mathbf{n}_A \otimes_S \mathbf{u}_A + \frac{1}{\theta_I}\, \mathbf{n}_M \otimes_S (\mathbf{u}_I - \mathbf{u}_{I-1}) \quad , I = 1 \ldots NV \tag{15}$$

with

$$\mathbf{a} \otimes_S \mathbf{b} := \frac{1}{2}\,(\mathbf{a} \otimes \mathbf{b} + \mathbf{b} \otimes \mathbf{a}) \tag{16}$$

$$\mathbf{u}_0 = \mathbf{0} \tag{17}$$

$$\mathbf{u}_{NV} = \mathbf{0} \tag{18}$$

as strain-states within each phase-domain. Obviously, the perturbed displacement-field is incompatible at the phase-interfaces. At this point, however, we assume that the lengthscale of higher order laminates is infinitely small compared to the one of lower order, which is suggested in [3]. Now, compatibility is satisfied in an averaged sense due to the fact that

$$\int \boldsymbol{\varepsilon}\,(\mathbf{x})\;\, dV = \theta_A\,\boldsymbol{\varepsilon}_A + \sum_{I=1}^{NV} \theta_I\,\boldsymbol{\varepsilon}_I = \boldsymbol{\varepsilon} \tag{19}$$

holds. With these definitions at hand, the averaged energy-density (6) can be rewritten as

$$\begin{aligned}\psi = {}& \frac{1}{2}\boldsymbol{\varepsilon} : \bar{\mathbf{C}} : \boldsymbol{\varepsilon} + \boldsymbol{\varepsilon} : [(\Delta\mathbf{C}\cdot\mathbf{n}_A)\cdot\mathbf{u}_A] + \frac{1}{2}\mathbf{u}_A\cdot\hat{\mathbf{C}}\cdot\mathbf{u}_A - \bar{\boldsymbol{\tau}} : \boldsymbol{\varepsilon} \\ & + \frac{1}{\theta_M}\,(\bar{\boldsymbol{\tau}}.\mathbf{n}_A)\cdot\mathbf{u}_A + \bar{\mathcal{C}} + \sum_{I=1}^{NV}\left\{\frac{1}{2\,\theta_I}\,(\mathbf{u}_I-\mathbf{u}_{I-1})\cdot\hat{\mathbf{C}}_M\cdot(\mathbf{u}_I-\mathbf{u}_{I-1})\right\} \\ & - \sum_{I=1}^{NV}\{\boldsymbol{\tau}_I\cdot(\mathbf{u}_I-\mathbf{u}_{I-1})\}\cdot\mathbf{n}_M\end{aligned} \tag{20}$$

where

$$\begin{aligned}\bar{\mathbf{C}} &:= \theta_A\,\mathbf{C}_A + \theta_M\,\mathbf{C}_M \\ \Delta\mathbf{C} &:= \mathbf{C}_A - \mathbf{C}_M \\ \tilde{\mathbf{C}} &:= \frac{1}{\theta_A}\,\mathbf{C}_A + \frac{1}{\theta_M}\,\mathbf{C}_M \\ \hat{\mathbf{C}} &:= \mathbf{n}_A\cdot\tilde{\mathbf{C}}\cdot\mathbf{n}_A = n_{A,i}\,\tilde{C}_{ijkl}\,n_{A,l}\,\mathbf{e}_j\,\mathbf{e}_k \\ \hat{\mathbf{C}}_M &:= \mathbf{n}_M\cdot\mathbf{C}_M\cdot\mathbf{n}_M = n_{M,i}\,C_{M,ijkl}\,n_{M,l}\,\mathbf{e}_j\,\mathbf{e}_k \\ \boldsymbol{\tau}_I &:= \boldsymbol{\varepsilon}_I^t : \mathbf{C}_M \qquad , I = 1\ldots NV \\ \bar{\boldsymbol{\tau}} &:= \sum_{I=1}^{NV}\theta_I\,\boldsymbol{\tau}_I \\ \bar{\mathcal{C}} &:= \theta_A\,\mathcal{C}_A + \theta_M\,\mathcal{C}_M + \frac{1}{2}\sum_{I=1}^{NV}\theta_I\,\boldsymbol{\tau}_I : \boldsymbol{\varepsilon}_I^t\end{aligned} \tag{21}$$

are used as abbreviations. In this sense, the underlying microstructure implicates $4\,NV + 6$ additional microstructural variables which are enlisted in

$$\mathcal{V} = (\theta_1, \theta_2, \ldots, \theta_{NV}, \mathbf{u}_A, \mathbf{u}_1, \mathbf{u}_2, \ldots, \mathbf{u}_{NV-1}, \mathbf{n}_A, \mathbf{n}_M) \quad . \tag{22}$$

A full relaxation given by minimizing out with respect to all internal variables, as in

$$\psi_{\mathrm{rel}}\,(\boldsymbol{\varepsilon}) = \min\{\psi; \mathcal{V}\} \tag{23}$$

would definitely result in the minimum energy-state of the material subjected to the underlying microstructure. However, this contradicts the hysteretic behavior of shape-memory alloys clearly indicating that dissipation has to be considered. One major aspect of our model is the differentiation of internal variables into elastic and inelastic ones. Note that the amplitudes of the perturbations $\mathbf{u}_A$, $\mathbf{u}_I$ are determined by purely elastic effects. Any change of their values will propagate with high velocity, namely the speed of sound. Hence, we choose the 'elastic variables' as

$$\mathcal{V}_{el} = (\mathbf{u}_A, \mathbf{u}_1, \mathbf{u}_2, \ldots, \mathbf{u}_{NV-1}) \tag{24}$$

In contrast any changes in the volume fractions $\theta_I$ or laminate orientations $\mathbf{n}_A$, $\mathbf{n}_M$ are associated with phase transformations and will cause dissipation leading to the choice of

$$\mathcal{V}_{\mathrm{diss}} = (\theta_1, \theta_2, \ldots, \theta_{NV}, \mathbf{n}_A, \mathbf{n}_M) \tag{25}$$

 

as 'inelastic' or 'dissipative variables'. This motivates a 'partial' relaxation of the underlying averaged energy-density as stated in

$$\psi_{\mathrm{rel}} = \min\left\{\psi; \mathcal{V}_{el}\right\} \qquad \text{subject to (9)} \tag{26}$$

yielding

$$\mathbf{u}_A^* = -\hat{\mathbf{C}}^{-1} \cdot \left(\Delta\mathbf{C} : \boldsymbol{\varepsilon} + \frac{1}{\theta_M}\bar{\boldsymbol{\tau}}\right) \cdot \mathbf{n}_A \tag{27}$$

$$\mathbf{u}_I^* = -\frac{1}{\theta_M}\hat{\mathbf{C}}_M^{-1} \cdot \left(\sum_{i=1}^{I}\sum_{j=I+1}^{NV}\left\{\theta_i\,\theta_j\,\left(\boldsymbol{\tau}_j - \boldsymbol{\tau}_i\right)\right\}\right) \cdot \mathbf{n}_M \tag{28}$$

as optimal amplitudes of the introduced perturbations. By substituting these results into (20) we finally obtain

$$\begin{aligned}\psi_{\mathrm{rel}}\left(\boldsymbol{\varepsilon}, \mathcal{V}_{\mathrm{diss}}\right) = {} & \frac{1}{2}\boldsymbol{\varepsilon} : \bar{\mathbf{C}} : \boldsymbol{\varepsilon} + \boldsymbol{\varepsilon} : \left[\left(\Delta\mathbf{C} \cdot \mathbf{n}_A\right) \cdot \mathbf{u}_A^*\right] + \frac{1}{2}\mathbf{u}_A^* \cdot \hat{\mathbf{C}} \cdot \mathbf{u}_A^* - \bar{\boldsymbol{\tau}} : \boldsymbol{\varepsilon} \\ & + \frac{1}{\theta_M}\left(\bar{\boldsymbol{\tau}} \cdot \mathbf{n}_A\right) \cdot \mathbf{u}_A^* - \frac{1}{2}\sum_{I=1}^{NV}\left\{\boldsymbol{\tau}_I \cdot \left(\mathbf{u}_I^* - \mathbf{u}_{I-1}^*\right)\right\} \cdot \mathbf{n}_M + \bar{\mathcal{C}}\end{aligned} \tag{29}$$

as relaxed energy-density, introducing the convention $\mathbf{u}_0^* = \mathbf{u}_{NV}^* = \mathbf{0}$[1]. This upper bound is in general not quasiconvex which means that the existence of minimizers of our variational problem is still not guaranteed and some residual fluctuations and mesh-dependency of numerical solutions may remain. But we expect our upper bound to be an approximation close enough to ensure that these effects are essentially negligible. In contrast to more accurate approximations of the quasiconvex hull, for example as stated in [15], Eq. (29) reflects a more efficient bound in terms of a rather straight-forward algorithmical treatment, as will be discussed in detail in Sect. 5. Taking the partial derivative of this functional with respect to the total strains results in effective stresses

$$\begin{aligned}\boldsymbol{\sigma} &= \frac{\partial\psi_{\mathrm{rel}}}{\partial\boldsymbol{\varepsilon}} \\ &= \bar{\mathbf{C}} : \boldsymbol{\varepsilon} - \boldsymbol{\varepsilon} : \left[\left(\Delta\mathbf{C} \cdot \mathbf{n}_A\right) \cdot \hat{\mathbf{C}}^{\text{-}1} \cdot \left(\mathbf{n}_A \cdot \Delta\mathbf{C}\right)\right] \\ &\quad - \frac{1}{\theta_M}\left(\Delta\mathbf{C} \cdot \mathbf{n}_A\right) \cdot \hat{\mathbf{C}}^{\text{-}1} \cdot \left(\bar{\boldsymbol{\tau}} \cdot \mathbf{n}_A\right) - \bar{\boldsymbol{\tau}}\ .\end{aligned} \tag{30}$$

Additionally, stress-like quantities

$$\mathbf{q} := -\frac{\partial\psi_{\mathrm{rel}}}{\partial\mathbf{p}} \tag{31}$$

can be determined which act as driving forces for the inelastic variables $\mathbf{p} \in \mathcal{V}_{\mathrm{diss}}$ and which will be extensively discussed in the following section. Since the analytic expressions of these quantities turn out to be quite extensive we omit their representation here.

## 4 Dissipation functionals and evolution equations

We have to adopt evolution laws for the remaining inelastic variables $\mathbf{p} \in \mathcal{V}_{\mathrm{diss}}$. For this purpose we adopt approaches from [33, 34, 36, 37]. Let us assume the existence of a dissipation functional $\Delta\left(\dot{\mathbf{p}}\right)$, as introduced for the first time in [12], giving the driving forces as

$$\mathbf{q} = \frac{\partial\Delta}{\partial\dot{\mathbf{p}}}. \tag{32}$$

Obviously, this evolution law can also be obtained by minimizing the sum of total power and dissipation functional $\dot{\psi}_{\mathrm{rel}} + \Delta$. In our case this leads to the consideration of a Lagrangian of the form

$$\mathcal{L} = \dot{\psi}_{\mathrm{rel}} + \boldsymbol{\Lambda} \cdot \dot{\mathbf{r}} + \Gamma\,\dot{\bar{r}} + \Delta\left(\dot{\mathbf{p}}\right) \quad , \tag{33}$$

[1] As already mentioned in (21), the symbol "·" means a single contraction of tensors with respect to neighboring indices.

 

because additionally we have to account for the restrictions (9) by introducing consistency parameters $\Lambda_I$ and $\Gamma$. In [16] formulations as the one given above are analyzed and shown to be (to a large extent) equivalent to the principle of maximum dissipation on the one hand and the minimization of the rate of free energy on the other hand. Minimizing $\mathcal{L}$ with respect to $\dot{\mathbf{p}}$ yields the stationarity conditions

$$\mathbf{0} \in \frac{\partial \mathcal{L}}{\partial \dot{\mathbf{p}}} = -\mathbf{q} + \frac{\partial \Delta}{\partial \dot{\mathbf{p}}} \tag{34}$$

where

$$q_I := -\frac{\partial \psi_{\mathrm{rel}}}{\partial \theta_I} + \Lambda_I - \Gamma \quad , I = 1 \dots NV \tag{35}$$

are redefined as extended driving forces for martensitic volume fractions. Eq. (34) may appear inconvenient because it gives the evolution of $\mathbf{p}$ only implicitly. Therefore the Legendre-Transform

$$J = \max \left\{ \mathbf{q} \cdot \dot{\mathbf{p}} - \Delta \left( \dot{\mathbf{p}} \right) ; \dot{\mathbf{p}} \right\} \tag{36}$$

is suggested, transforming (34) into

$$\dot{\mathbf{p}} \in \frac{\partial J}{\partial \mathbf{q}} \tag{37}$$

where the dual inelastic potential $J$ has been introduced. In this context, a dissipation functional $\Delta$ chosen to be homogeneous of first order will always lead to an indicator function

$$J = \begin{cases} 0 & , \text{if } \Phi \leq 0 \\ \infty & , \text{else} \end{cases} \tag{38}$$

with $\Phi$ as generalized characteristic function to separate elastic from inelastic behavior.

The model will now be specified under the assumption of constant laminate orientations $\mathbf{n}_A$, $\mathbf{n}_M$. This assumption seems to be realistic, because the rotation of the laminate-microstructure would require a large scale redistribution of variants being associated with high dissipation. Such rotations are to our knowledge not observed in experiments either. Hence, only the volume fractions $\theta_I$ remain as internal inelastic variables of the model. Let us consider the following three examples[2]:

$$\Delta = k \left\| \dot{\boldsymbol{\theta}} \right\| \tag{39}$$

$$\Delta = k \sum_{I=1}^{NV} |\dot{\theta}_I| \tag{40}$$

$$\Delta = k_1 \sum_{I=1}^{NV} |\dot{\theta}_I| + k_2 \left\| \dot{\boldsymbol{\theta}} \right\|^2 \tag{41}$$

with

$$\left\| \dot{\boldsymbol{\theta}} \right\| = \sqrt{\sum_{I=1}^{NV} \dot{\theta}_I^2} \, . \tag{42}$$

In Table 1 we provide an overview of the evolution-laws determined via (37) and corresponding to the dissipation potentials (39), (40), (41). They are characterized by the system of ordinary differential equations (ODE) and consistency conditions (CONS). We also give the type of inelastic evolution obtained (von Mises, Tresca, Perzyna). The derivations are lengthy but straight-forward. In the case of viscoplastic evolution, $\langle \Phi_I \rangle$ denotes the so called ramp-function according to [44], which will be defined as

$$\langle \Phi_I \rangle := \max \left\{ \Phi_I, 0 \right\} = \frac{1}{2} \left( 1 + \operatorname{sign} \left( \Phi_I \right) \right) \, \Phi_I \, . \tag{43}$$

Obviously, the parameters $k$, $k_1$ act as threshold values whereas $k_2$ can be regarded as a measure of viscosity.

[2] We omit here considering dissipation potentials of the form $\Delta = k \left\| \dot{\boldsymbol{\theta}} \right\| + k_2 \left\| \dot{\boldsymbol{\theta}} \right\|^2$ because it does not provide much new information.

 

**Table 1** Yield functions ($\Phi$), evolution equations (ODE), and consistency conditions (CONS) for specific choices of $\Delta$.

| $\Delta$ | $\Phi$ | ODE | CONS | Type |
|---|---|---|---|---|
| (39) | $\|\mathbf{q}\| - k$ | $\dot{\theta}_I = \lambda \, \frac{q_I}{\|\mathbf{q}\|}$ | $\Phi \, \lambda = 0$<br>$\Phi \leq 0$<br>$\lambda \geq 0$ | von Mises |
| (40) | $\|q_I\| - k \, , I = 1...NV$ | $\dot{\theta}_I = \lambda_I \, \text{sign}\,(q_I)$ | $\Phi_I \, \lambda_I = 0$<br>$\Phi_I \leq 0$<br>$\lambda_I \geq 0$ | Tresca |
| (41) | $\|q_I\| - k_1 \, , I = 1...NV$ | $\dot{\theta}_I = \frac{1}{2\,k_2} \, \text{sign}\,(q_I) \, \langle \Phi_I \rangle$ | none | Perzyna |

## 5 Algorithmical treatment

Let us now elaborate on the algorithmical treatment of the evolution-laws derived above. As mentioned before, we consider the laminate orientations $\mathbf{n}_A$ and $\mathbf{n}_M$ to be fixed during microstructure evolution. However, their values need to be specified, which is achieved by treating these vectors as minimizers of $\psi_{\text{rel}}$ as long as the material response is elastic. During phase transformations the values are then kept constant. In case of von Mises- and Tresca-type evolution, the presence of consistency conditions causes the now differential-algebraic system of equations to become 'stiff'. Thus, an A- and L-stable numerical scheme is required. Here we make use of a classical Backward-Euler scheme. In this sense, time-discretized evolution equations are given by

$$\theta_I - \theta_I^{n-1} - \Delta\lambda \, \frac{q_I}{\|\mathbf{q}\|} = 0 \qquad \text{von Mises-type} \tag{44}$$

$$\theta_I - \theta_I^{n-1} - \Delta\lambda_I \, \text{sign}\,(q_I) = 0 \qquad \text{Tresca-type} \tag{45}$$

$$\theta_I - \theta_I^{n-1} - \frac{\Delta t}{4\,k_2} \, \text{sign}\,(q_I) \, (1 + \text{sign}\,(\Phi_I)) \, \Phi_I = 0 \qquad \text{Perzyna-type} \tag{46}$$

for each volume fraction of martensite[3], where $\Delta\lambda := \lambda \, \Delta t$. Inequality constraints like the consistency conditions stated in Table 1 always mean a challenge in the context of algorithmical implementation. Since we have to deal with several phase fractions, whose evolution is strongly coupled, the application of standard predictor-corrector methods is not suitable, because an elaborate active set search has to be carried out. Iterative solution procedures then suffer from instabilities caused by periodic oscillations of the active set. A more effective way was introduced in [40] in the context of crystal plasticity. There, an augmented Lagrangian approach is suggested replacing the set of Kuhn-Tucker conditions $\Phi \, \Delta\lambda = 0$, $\Phi \leq 0$, $\Delta\lambda \geq 0$ by the so-called Fischer-Burmeister complementary functions

$$\sqrt{\Phi^2 + \Delta\lambda^2} + \Phi - \Delta\lambda = 0. \tag{47}$$

The same strategy can be employed in order to treat the set of inequalities given by (9). Taking into account the corresponding parameters $\Lambda_I$ and $\Gamma$ introduced in (33) one obtains additional Kuhn-Tucker conditions

$$r_I \, \Lambda_I = 0, \quad r_I \leq 0, \quad \Lambda_I \geq 0 \tag{48}$$

and

$$\bar{r} \, \Gamma = 0, \quad \bar{r} \leq 0, \quad \Gamma \geq 0 \, . \tag{49}$$

We may now substitute (48) and (49) by the equalities

$$\sqrt{r_I^2 + \Lambda_I^2} + r_i - \Lambda_I = 0 \, , \tag{50}$$

$$\sqrt{\bar{r}^2 + \Gamma^2} + \bar{r} - \Gamma = 0 \, . \tag{51}$$

[3] Similar formulations may be employed in order to derive evolution equations for the laminate orientations.

It is well-known that algorithms based on the Fischer-Burmeister complementary functions are numerically sensitive. However, their application leads to rather well-behaved schemes here. We can summarize now: the incremental update of the microstructure within a time-step is achieved by solving one of the Eqs. (44), (45), (46) (depending on the type of evolution) along with (50) and (51). In the case of von Mises- or Tresca-type evolution (47) has to be solved in addition. Note that no inequality constraints are present and no active set search is required anymore.

## 6 Material point computations

To emphasize the multifunctionality of the presented model several microscopic analyses are performed. In this regard, material parameters and transformation strains are chosen as stated in Appendices A and B, respectively, the latter depending on the different materials under consideration. Further parameters are chosen as $\mathcal{C}_A = 0\,\mathrm{MPa}$, $\mathcal{C}_M = 0.25\,\mathrm{MPa}$, and $k = 1.25\,\mathrm{MPa}$.

In the case of Tresca-type evolution-laws, Figs. 4 and 5 depict the behavior of a material undergoing cubic-tetragonal transformations subjected to uniaxial tension

$$\boldsymbol{\varepsilon} = \kappa\,(t) \begin{pmatrix} 0.025 & 0 & 0 \\ 0 & 0 & 0 \\ 0 & 0 & 0 \end{pmatrix} \tag{52}$$

introducing the time-dependent global load factor $\kappa$, which was initially increased from $0$ to $1$, subsequently decreased to $-0.85$ and finally raised to $0$ again providing a full load-cycle. We obtain almost perfect stress-plateaus at different levels revealing a tension-compression asymmetry verified by numerous experimental observations. We would like to emphasize here that this is achieved in a natural way without assuming different yield limits. The reason for this behavior lies in the evolution of different martensitic variants. In tension, there is only one preferred martensitic crystal structure, namely variant $1$, whereas in compression both variants $2$ and $3$ develop simultaneously. Fig. 6 underlines the effect of the energy-relaxation concept: A significant reduction of the original functional is achieved in those areas where it appears to be non-quasiconvex. It should also be noted here that phase-energy densities of variants $2$ and $3$ cannot be distinguished in Fig. 6 because of their equality.

An applied torsion

$$\boldsymbol{\varepsilon} = \kappa\,(t) \begin{pmatrix} 0 & 0 & 0 \\ 0 & 0 & 0.02 \\ 0 & 0.02 & 0 \end{pmatrix} \tag{53}$$

with $\kappa$ alternating between $-1$ and $1$ results in the behavior shown in Figs. 7 and 8. In this case, none of the variants is preferred and hence all of them develop equally causing a symmetric stress-strain relationship.

Similar results obtained in the case of a cubic-orthorhombic transformation are depicted in Figs. 9 to 12. It is noteworthy to mention here, that we use identical material parameters independent of the underlying transformation mode. Of course, the assumption of isotropy is neither valid for any martensitic crystal structure nor for austenite. For example in the case of cubic-orthorhombic transformations [41] provides values for the elastic stiffnesses of CuAlNi. However, we still treat the material as isotropic since such values are in general hardly available or differ significantly throughout the literature. As an additional aspect, this enables us to compare different transformation-modes just in terms of the underlying Bain-strains. The results shown in Figs. 9 to 12 are incidentally obtained for $k = 5\,\mathrm{MPa}$.

The stress-strain diagram shown in Fig. 9 resulting from an applied uniaxial tension of the form

$$\boldsymbol{\varepsilon} = \kappa\,(t) \begin{pmatrix} 0.055 & 0 & 0 \\ 0 & 0 & 0 \\ 0 & 0 & 0 \end{pmatrix} \tag{54}$$

where $\kappa$ ranges from $-1.0$ to $1.0$ reveals deviations from plateaus of constant stress during phase-transformations. In tension, elastic stresses slightly increase while martensitic volume fractions change, whereas in compression the most significant difference to the cubic-tetragonal mode is a 'kinked' path at the beginning of re-transformation from martensite to austenite, which is also present in tension but not that pronounced. This phenomenon is caused by changes regarding the evolution of volume fractions of martensite depicted in Fig. 10, where variants 2, 4, and 6 always coexist during the whole load-cycle. Plateau-stresses are significantly higher compared to those for tetragonal martensitic systems. This shows that

 

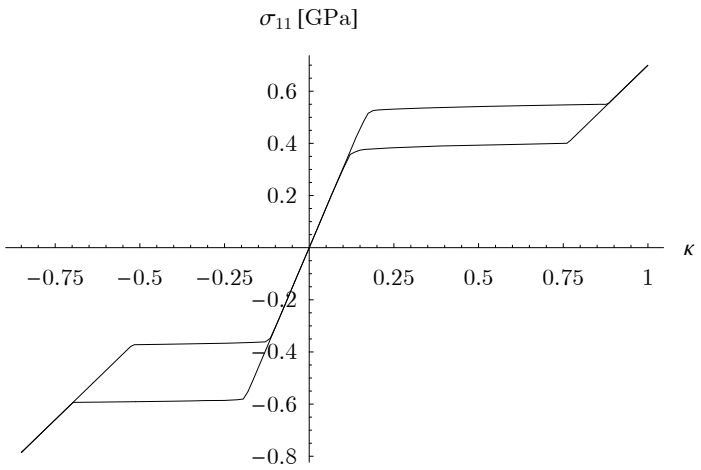


**Fig. 4** Applying uniaxial tension to a cubic-tetragonal system with an underlying Tresca-type evolution law results in almost perfect stress-plateaus with a pronounced tension-compression asymmetry achieved in a natural way

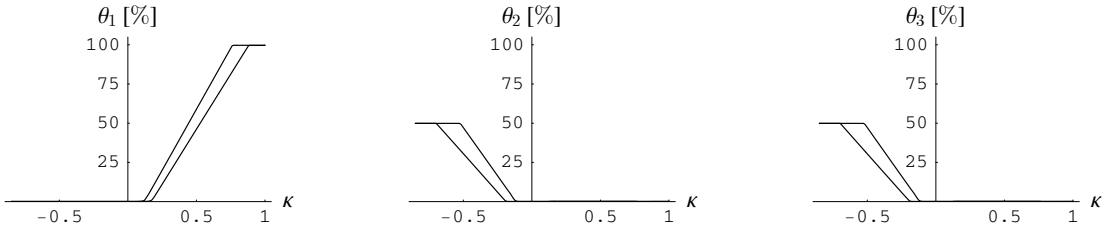


**Fig. 5** The asymmetry between tension and compression is due to the evolution of different martensitic variants, where in compression variants 2 and 3 coexist and evolve simultaneously

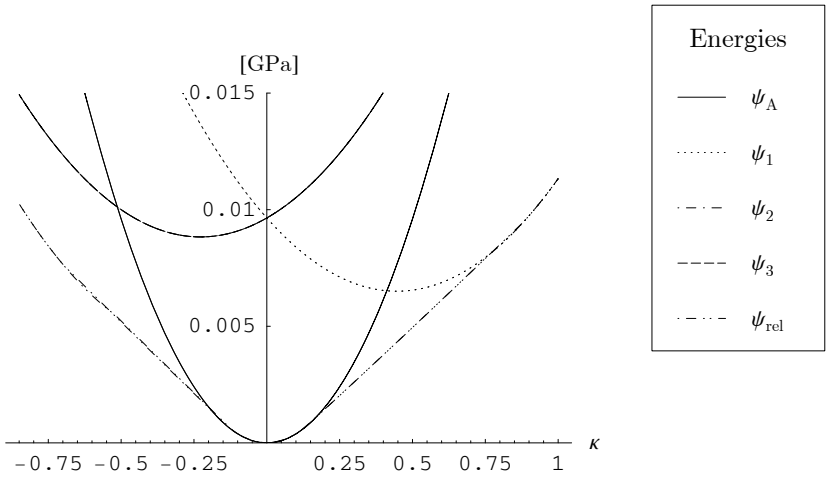


**Fig. 6** Phase-mixtures cause a significant relaxation of energy characterized by the specific hull $\psi_{\mathrm{rel}}$ (cubic-tetragonal, uniaxial tension, Tresca-type evolution)

applied tension is rather unfavorable for this kind of transformation. Contrarily, applied torsional deformations like

$$\varepsilon = \kappa(t) \begin{pmatrix} 0 & 0 & 0 \\ 0 & 0 & 0.045 \\ 0 & 0.045 & 0 \end{pmatrix} \tag{55}$$

cause much earlier initiations of phase-transitions as can be seen in Fig. 11. In this case, the symmetry of tension and compression is present again and also recognizable by the evolution of martensitic volume fractions shown in Fig. 12.

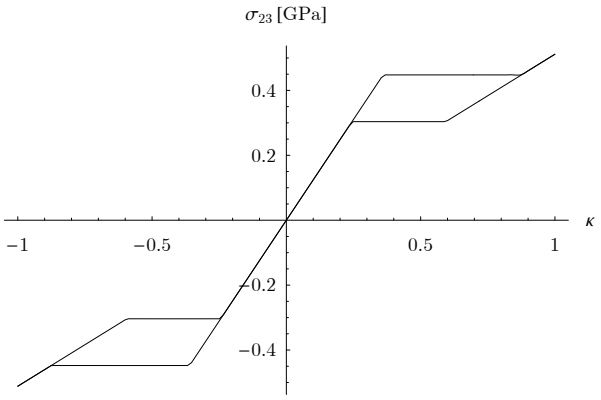


**Fig. 7** Torsional loads appear to be more 'favorable' for phase-transitions and moreover lead to a symmetric material response in case of cubic-tetragonal transformations. The underlying evolution law is of Tresca-type here.

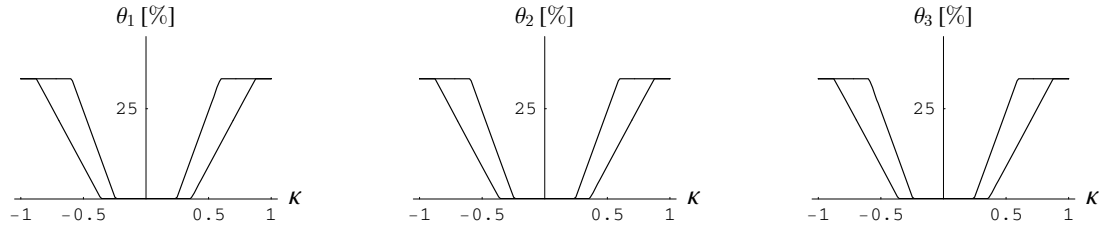


**Fig. 8** The evolution of phase fractions show that in case of simple shear no preferred tetragonal variant exists.

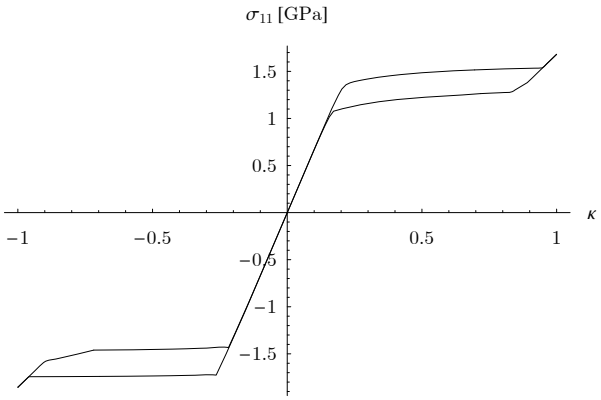


**Fig. 9** The material behavior of cubic-orthorhombic systems under applied uniaxial tension with an underlying Tresca-type evolution law differs from tetragonal martensites: transformation stresses are higher, in tension there is no 'perfect' stress plateau and in compression a pronounced 'kink' of the stress-strain curve is present

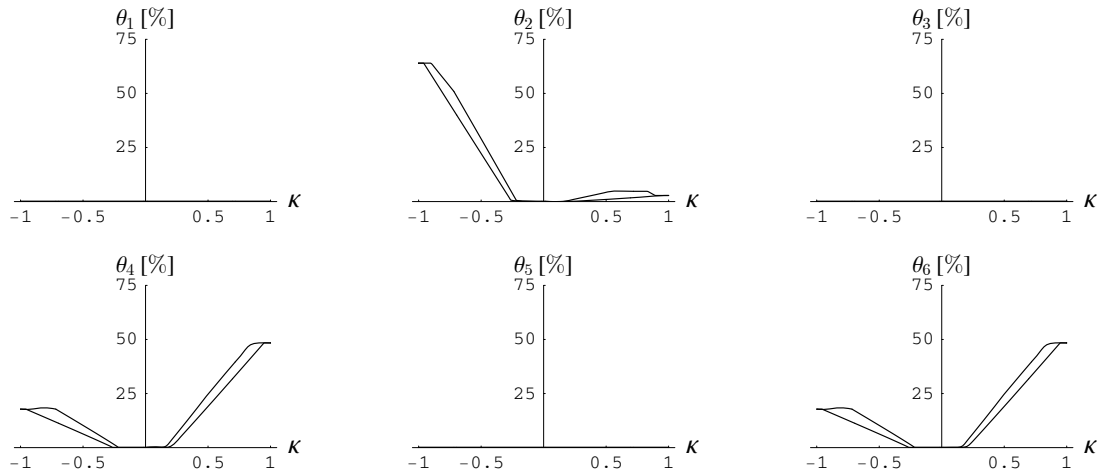


**Fig. 10** The evolution of martensitic variants again shows asymmetry between tension and compression. Variants 1, 3 and 5 are completely unaffected.

 

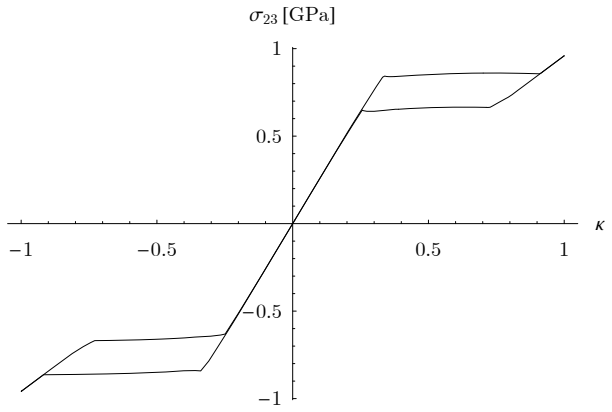


**Fig. 11** Applied shear loads again result in a symmetric material response. Moreover, phase-transitions occur much earlier for orthorhombic martensites compared to uniaxial tension as well. The underlying evolution law is of Tresca-type here.

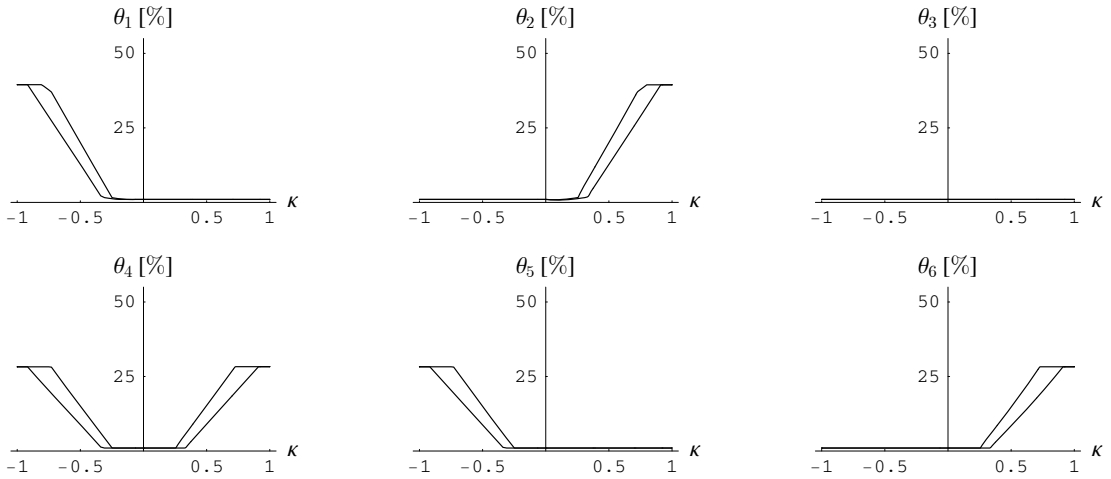


**Fig. 12** Like the stress-strain relation, the evolution of volume fractions exhibits symmetry between tension and compression, where only variant 3 never shows up and always 3 variants coexist

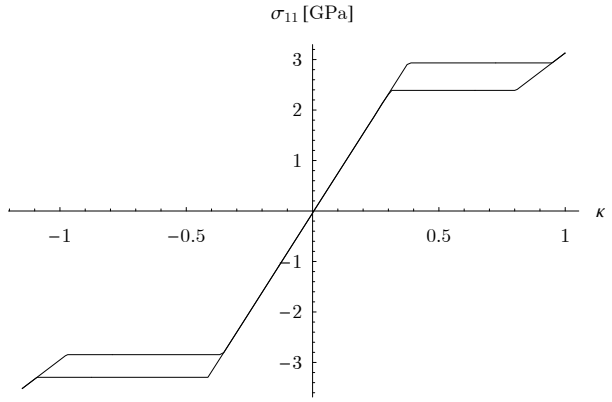


**Fig. 13** Monoclinic systems appear to be most unfavorable under applied uniaxial tension. The stress-strain curve is characterized by sharp transitions which is not valid for other transformation modes. Here, a Tresca-type evolution law has been applied.

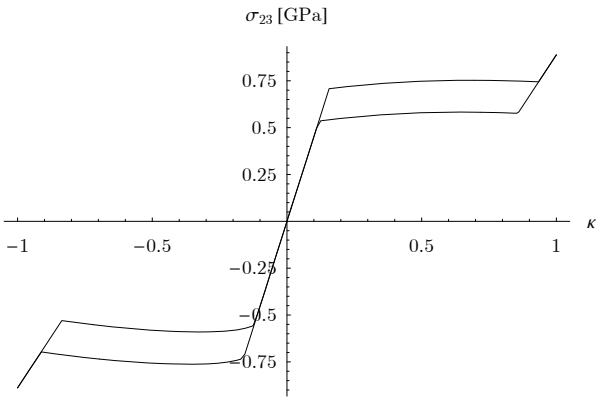


**Fig. 14** Subjected to simple shear for the Tresca-type evolution law, monoclinic systems only show nearly symmetric behavior in tension and compression. Moreover, decreasing stresses are revealed which, however, does not contradict the concept of energy-relaxation

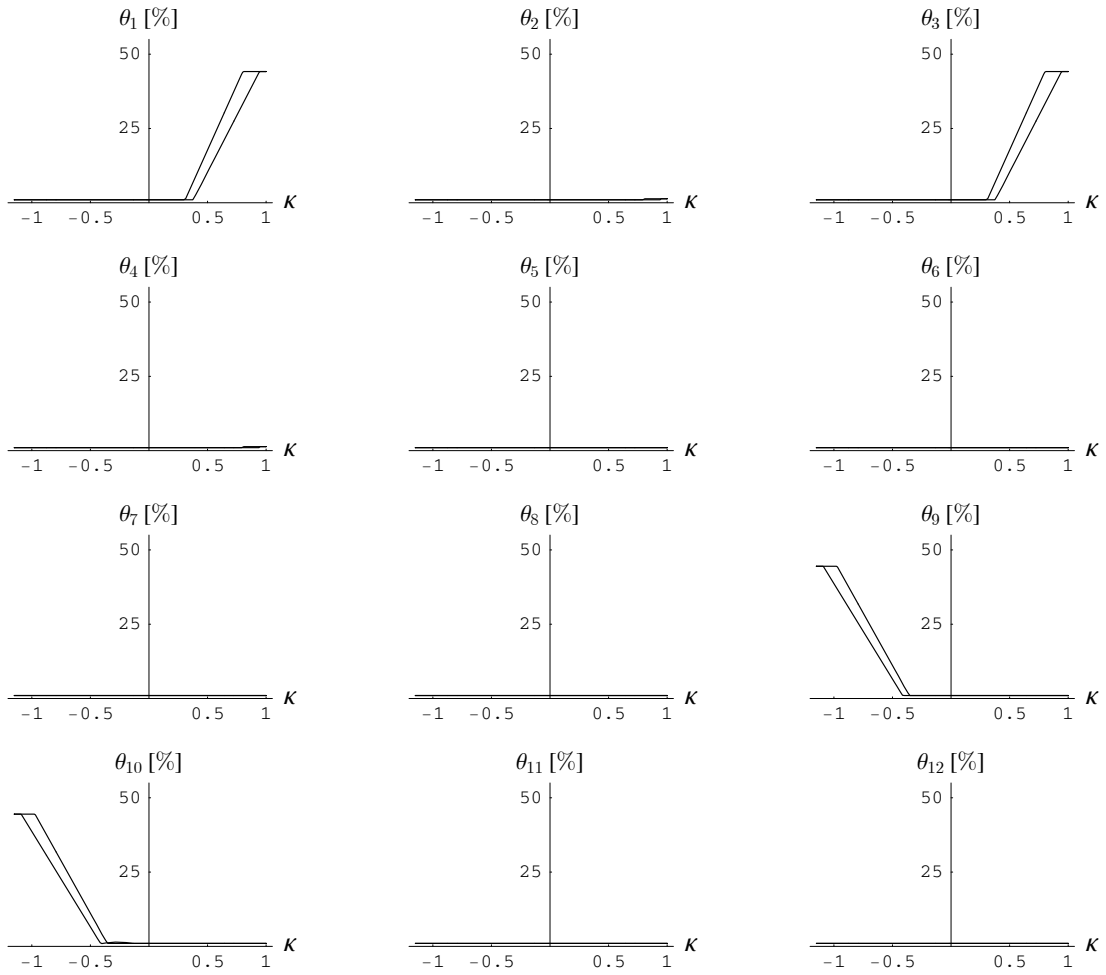


**Fig. 15** Although monoclinic systems offer 12 possible martensitic variants only 2 of them evolve simultaneously.

Even though a monoclinic crystallographic system exhibits 12 possible variants of martensite, only 2 of them show up at the same time under applied uniaxial tension of the form

$$\boldsymbol{\varepsilon} = \kappa\,(t) \begin{pmatrix} 0.075 & 0 & 0 \\ 0 & 0 & 0 \\ 0 & 0 & 0 \end{pmatrix} \tag{56}$$

with $\kappa \in [-1.15, 1.0]$ (see Fig. 15). The stress-plateaus depicted in Fig. 13 are characterized by the highest stresses of all examples considered. Like in all other examples, phase-transitions are initiated much earlier if the material is subjected to shear like

$$\boldsymbol{\varepsilon} = \kappa\,(t) \begin{pmatrix} 0 & 0 & 0 \\ 0 & 0 & 0.085 \\ 0 & 0.085 & 0 \end{pmatrix} \tag{57}$$

with $\kappa \in [-1.0, 1.0]$ (see Fig. 14). Interestingly, again only two coexisting martensitic variants are present as depicted in Fig. 16. As a marginal note it should be mentioned, that the presented results for monoclinic martensites are obtained for $k = 12.5\,\mathrm{MPa}$. Fig. 14 additionally reveals an interesting feature of the model, namely that the material response exhibits decreasing stresses during phase-transformations. This is due to the fact that the applied load does not correspond to a rank-one direction (like uniaxial tension) and moreover, the underlying relaxed energy hull generally lies above the rank-1-convex one, see [9] for instance. Hence, the relaxed energy density does not need to be convex and accordingly stresses can decrease in general without losing physical integrity.

 

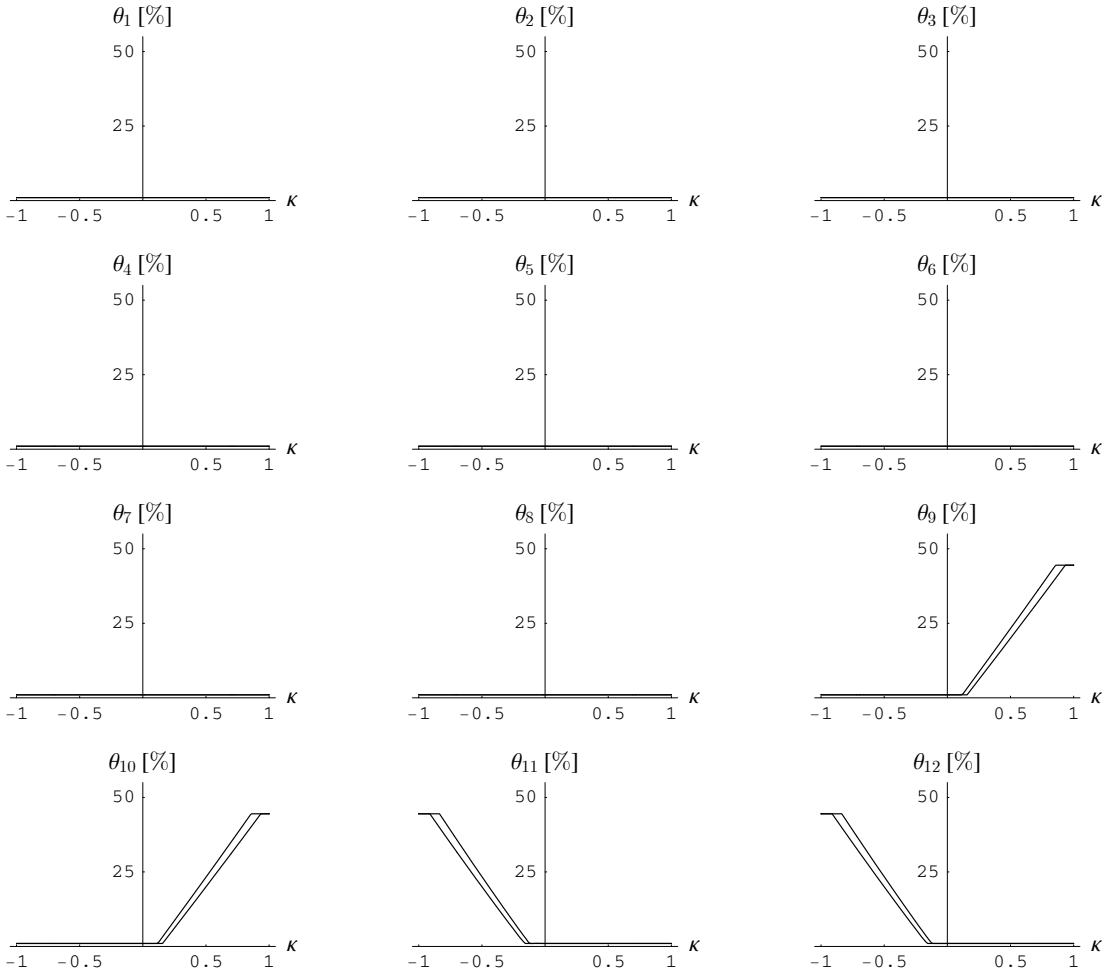


**Fig. 16** Like under applied tension, only 2 out of 12 possible variants evolve in each 'load-direction'. The slight deviations in terms of tension-compression symmetry are hardly visible when considering the evolution of phase-fractions.

In case of von Mises- and Perzyna-type evolution laws, Fig. 17 shows stress-strain diagrams for each type of evolution under applied uniaxial deformations equivalent to (52) for three-variant martensite. Since only one variant is preferred in tension at least except the end of the stress-plateau, von Mises- and Tresca-type evolution coincide. The fact that in case of von Mises-type evolution small amounts of variant 2 and 3 show up (see Fig. 18) causes a slight deviation. The additional viscous terms within the Perzyna-type modelling naturally result in larger hysteresis loops. Here, the viscosity coefficient was chosen to be $k_2 = 0.625\,\mathrm{MPa/s}$. The effect of the specific value for this parameter on effective stresses and the evolution of phase-fractions is depicted in Figs. 19 and 20, respectively. Due to the fact that evolving volume fractions are penalized differently in the framework of each evolution-law, even von Mises- and Tresca-type evolutions differ from each other in compression, where two variants coexist in any case.

Referring to the 'viscoplastic' evolution law once again, Figs. 21 and 22 clarify its rate-dependent character. These results are obtained by applying the same load-conditions as before, where the complete load-path has been divided into several increments as well as those being divided into several time-increments while keeping the load constant. This procedure results in instantaneously increasing stress after every new load-step whereas volume fractions of martensite are unaffected at first. Subsequently in the case of growing martensites, the phase-front is accelerated leading to a smooth relaxation of stress and increase of volume fractions. The dotted lines in Figs. 21 and 22 symbolize the solution at the end of each time interval between load-increments.

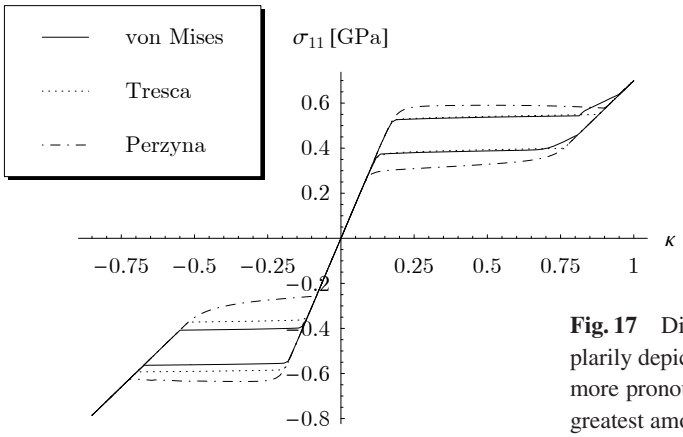


**Fig. 17** Different evolution laws result in different material behavior (exemplarily depicted for applied uniaxial load of tetragonal martensites), which is more pronounced in compression. Perzyna-type evolution always yields the greatest amount of dissipation due to the additional viscoplastic terms.

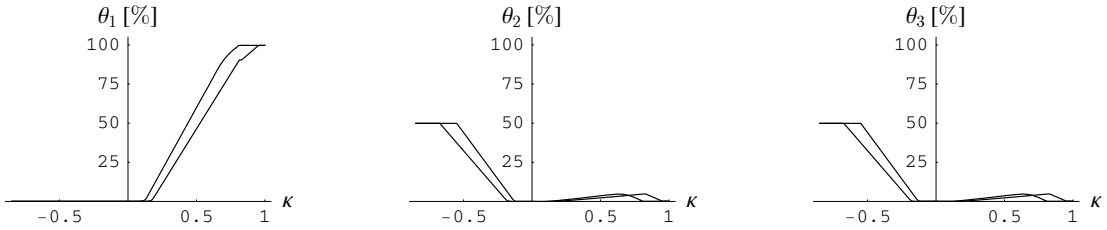


**Fig. 18** Compared to Fig. 4, the evolution of volume fractions for von Mises-type evolution shows slight deviations.

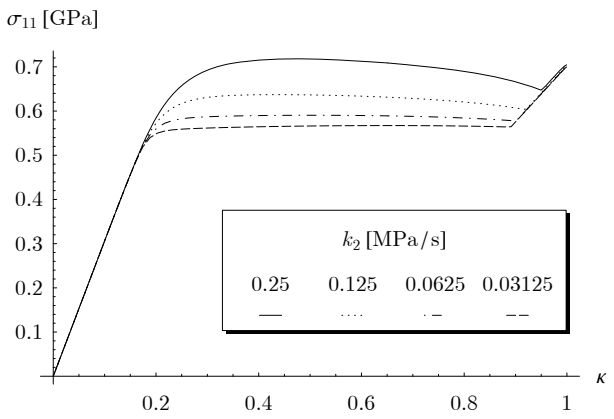


**Fig. 19** Higher values of the 'viscosity coefficient' $k_2$ result in higher stresses provided that the rate of loading is chosen high enough to prevent their relaxation.

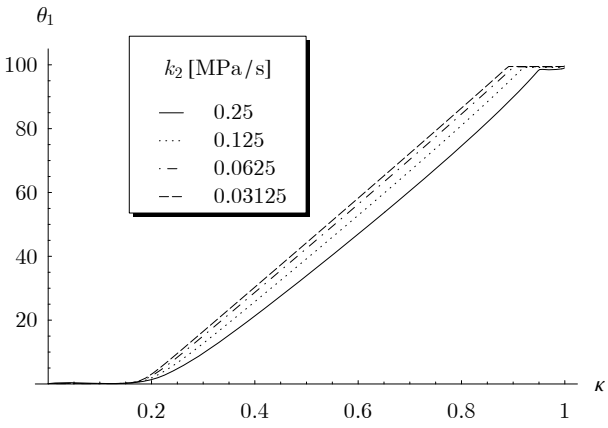


**Fig. 20** Accordingly, higher values of $k_2$ also cause a 'damped' and 'smoothened' evolution of volume fractions.

## 7 Conclusions

The presented results confirm that the concept of energy-relaxation combined with evolution-laws derived from inelastic potentials provides an effective tool for the modelling of inelastic materials, especially under consideration of induced microstructures. In this context, material models designed to approximate the quasiconvex hull of an underlying energy-density of a phase mixture are based on a solid foundation from the viewpoint of mathematics as well as physics.

Concerning the question, which of the evolution-laws turns out to be most suitable, the numerical analyses can hardly provide any clue. It's rather up to the physical interpretation of each of them to answer this question. In this regard, von Mises-type evolution is rather arguable since driving forces of each phase affect the evolution of all other ones. Even though we do not exceed the boundaries of quasistatics, Perzyna-type evolution accounts for the fact that phase-fronts evolve with

 

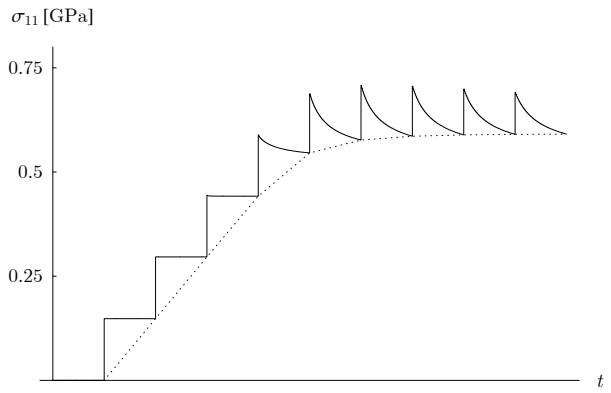


**Fig. 21** Keeping the load piecewise constant for a certain period of time shows the 'viscoplastic effect': stresses are raised instantly after each load-increment and relax afterwards due to the propagation of phases.

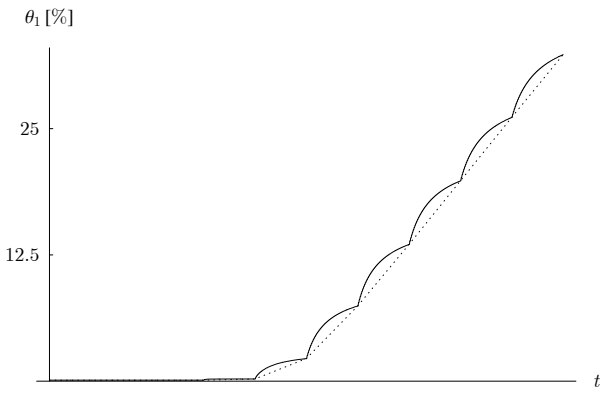


**Fig. 22** In contrast to elastoplastic evolution laws, volume fractions within a Perzyna-type framework remain unchanged after a load-increment is applied. Subsequently, they evolve with finite velocity and converge to the 'elastoplastic solution'.

finite velocities in contrast to rate-independent von Mises- and Tresca-type evolution. This 'time-dependent' behavior of evolving phase-fractions appears to be more realistic.

Due to the fact that all relevant quantities like stresses and driving forces can be stated in analytical form, the extension of the model in terms of FE-implementation appears to be promising. Hence, this is going to be a major topic of our forthcoming research activities.

## A Transformation matrices

In the context of this appendix we refer to [5] and the references mentioned therein, respectively, as source for the applied values of transformation strains depending on the underlying material.

### A.1 Cubic to tetragonal transformation (InTl)

$$\mathbf{U}_1 = \begin{pmatrix} \beta & 0 & 0 \\ 0 & \alpha & 0 \\ 0 & 0 & \alpha \end{pmatrix}, \mathbf{U}_2 = \begin{pmatrix} \alpha & 0 & 0 \\ 0 & \beta & 0 \\ 0 & 0 & \alpha \end{pmatrix}, \mathbf{U}_3 = \begin{pmatrix} \alpha & 0 & 0 \\ 0 & \alpha & 0 \\ 0 & 0 & \beta \end{pmatrix} \tag{58}$$

with $\alpha = 0.9889, \beta = 1.0221$.

### A.2 Cubic to orthorhombic transformation (CuAlNi)

$$\begin{aligned} \mathbf{U}_1 &= \begin{pmatrix} \frac{\alpha+\gamma}{2} & 0 & \frac{\alpha-\gamma}{2} \\ 0 & \beta & 0 \\ \frac{\alpha-\gamma}{2} & 0 & \frac{\alpha+\gamma}{2} \end{pmatrix}, \mathbf{U}_2 = \begin{pmatrix} \frac{\alpha+\gamma}{2} & 0 & \frac{\gamma-\alpha}{2} \\ 0 & \beta & 0 \\ \frac{\gamma-\alpha}{2} & 0 & \frac{\alpha+\gamma}{2} \end{pmatrix}, \mathbf{U}_3 = \begin{pmatrix} \frac{\alpha+\gamma}{2} & \frac{\alpha-\gamma}{2} & 0 \\ \frac{\alpha-\gamma}{2} & \frac{\alpha+\gamma}{2} & 0 \\ 0 & 0 & \beta \end{pmatrix} \\ \mathbf{U}_4 &= \begin{pmatrix} \frac{\alpha+\gamma}{2} & \frac{\gamma-\alpha}{2} & 0 \\ \frac{\gamma-\alpha}{2} & \frac{\alpha+\gamma}{2} & 0 \\ 0 & 0 & \beta \end{pmatrix}, \mathbf{U}_5 = \begin{pmatrix} \beta & 0 & 0 \\ 0 & \frac{\alpha+\gamma}{2} & \frac{\alpha-\gamma}{2} \\ 0 & \frac{\alpha-\gamma}{2} & \frac{\alpha+\gamma}{2} \end{pmatrix}, \mathbf{U}_6 = \begin{pmatrix} \beta & 0 & 0 \\ 0 & \frac{\alpha+\gamma}{2} & \frac{\gamma-\alpha}{2} \\ 0 & \frac{\gamma-\alpha}{2} & \frac{\alpha+\gamma}{2} \end{pmatrix} \end{aligned} \tag{59}$$

with $\alpha = 1.0619, \beta = 0.9278, \gamma = 1.0230$.

### A.3 Cubic to monoclinic(I) transformation (NiTi)

$$
\begin{aligned}
\mathbf{U}_1 &= \begin{pmatrix} \alpha & \delta & \epsilon \\ \delta & \alpha & \epsilon \\ \epsilon & \epsilon & \beta \end{pmatrix}, \mathbf{U}_2 = \begin{pmatrix} \alpha & \delta & -\epsilon \\ \delta & \alpha & -\epsilon \\ -\epsilon & -\epsilon & \beta \end{pmatrix}, \mathbf{U}_3 = \begin{pmatrix} \alpha & -\delta & -\epsilon \\ -\delta & \alpha & \epsilon \\ -\epsilon & \epsilon & \beta \end{pmatrix} \\
\mathbf{U}_4 &= \begin{pmatrix} \alpha & -\delta & \epsilon \\ -\delta & \alpha & -\epsilon \\ \epsilon & -\epsilon & \beta \end{pmatrix}, \mathbf{U}_5 = \begin{pmatrix} \alpha & \epsilon & \delta \\ \epsilon & \beta & \epsilon \\ \delta & \epsilon & \alpha \end{pmatrix}, \mathbf{U}_6 = \begin{pmatrix} \alpha & -\epsilon & \delta \\ -\epsilon & \beta & -\epsilon \\ \delta & -\epsilon & \alpha \end{pmatrix} \\
\mathbf{U}_7 &= \begin{pmatrix} \alpha & -\epsilon & -\delta \\ -\epsilon & \beta & \epsilon \\ -\delta & \epsilon & \alpha \end{pmatrix}, \mathbf{U}_8 = \begin{pmatrix} \alpha & \epsilon & -\delta \\ \epsilon & \beta & -\epsilon \\ -\delta & -\epsilon & \alpha \end{pmatrix}, \mathbf{U}_9 = \begin{pmatrix} \beta & \epsilon & \epsilon \\ \epsilon & \alpha & \delta \\ \epsilon & \delta & \alpha \end{pmatrix} \\
\mathbf{U}_{10} &= \begin{pmatrix} \beta & -\epsilon & -\epsilon \\ -\epsilon & \alpha & \delta \\ -\epsilon & \delta & \alpha \end{pmatrix}, \mathbf{U}_{11} = \begin{pmatrix} \beta & -\epsilon & \epsilon \\ -\epsilon & \alpha & -\delta \\ \epsilon & -\delta & \alpha \end{pmatrix}, \mathbf{U}_{12} = \begin{pmatrix} \beta & \epsilon & -\epsilon \\ \epsilon & \alpha & -\delta \\ -\epsilon & -\delta & \alpha \end{pmatrix}
\end{aligned}
\tag{60}
$$

with $\alpha = 1.0243, \beta = 0.9563, \delta = 0.058, \epsilon = 0.0427$.

## B Material parameters

As stated in this paper already, the applied values for the elastic properties of both austenite and martensite lack of physical motivation. However, since the scope of this paper is to present the general concept of energy-relaxation as a sophisticated method for the modelling of inelastic materials we adopt values exemplarily provided at [31] for NiTi, namely

$$
\begin{aligned}
\text{Young's modulus of austenite} &: E_A = 83.0\,\text{GPa}\,, \\
\text{Young's modulus of martensite} &: E_M = 34.0\,\text{GPa}\,, \\
\text{Poisson's ratio of austenite} &: \nu_A = 0.33\,, \\
\text{Poisson's ratio of martensite} &: \nu_M = 0.33\,.
\end{aligned}
$$

## References


[1] F. Auricchio and R. Taylor, Shape-memory alloys: modelling and numerical simulations of the finite-strain superelastic behavior, Comp. Meth. Appl. Mech. Engrg. **143**, 175–194 (1997).
[2] E. C. Bain, Trans. AIME **70**, 25–46 (1924).
[3] J. Ball and R. James, Fine phase mixtures as minimizers of energy, Arch. Rat. Mech. Anal. **100**, 13–52 (1987).
[4] T. Bartel and K. Hackl, A novel approach to the modelling of single–crystalline materials undergoing martensitic phase–transformations, Mat. Sc. Engrg. A **481–482**, 371–375 (2006).
[5] K. Bhattacharya, Microstructure of Martensite – Why it forms and how it gives rise to the shape-memory effect (Oxford University Press, New York, 2003).
[6] C. Carstensen, K. Hackl, and A. Mielke, Nonconvex potentials and microstructures in finite-strain plasticity, Proc. Roy. Soc. London A **458**, 299–317 (2002).
[7] C. Carstensen and P. Plechac, Numerical analysis of a relaxed variational model of hysteresis in two-phase solids, Math. Model. Numer. Anal. **35**, 865–878 (2001).
[8] S. Conti, Branched microstructures: Scaling and asymptotic self–similarity, Comm. Pure Appl. Mech. **53**, 1448–1474 (2000).
[9] B. Dacorogna, Quasiconvexity and relaxation of the nonconvex problems in the calculus of variations, J. Funct. Anal. **46**, 102–118 (1982).
[10] A. DeSimone and G. Dolzmann, Material instabilities in nematic polymers, Physica D **136**, 175–191 (1999).
[11] A. DeSimone and G. Dolzmann, Macroscopic response of nematic elastomers via relaxation of a class of SO(3)-invariant energies, Arch. Rat. Mech. Anal. **161**, 181–204 (2002).
[12] D. G. B. Edelen, On the existence of symmetry relations and dissipation potentials, Arch. Rat. Mech. Anal. **51**, 218–227 (1973).
[13] S. Govindjee, K. Hackl, and R. Heinen, An upper bound to the free energy of mixing by twin-compatible lamination for $n$-variant martensitic phase transformations, Continuum Mech. Thermodyn. **18**, 443–453 (2007).
[14] S. Govindjee and C. Miehe, A multi-variant martensitic phase transformation model: formulation and numerical implementation, Comp. Methods Appl. Mech. Engrg. **191**, 215–238 (2001).


 

[15] S. Govindjee, A. Mielke, and G. Hall, The free energy of mixing for $n$-variant martensitic phase transformations using quasi-convex analysis, J. Mech. Phys. Sol. **50**, 1897–1922 (2002).
[16] K. Hackl and F. D. Fischer, On the relation between the principle of maximum dissipation and inelastic evolution given by dissipation potentials, Proc. Roy. Soc. A **464**, 117–132 (2008).
[17] K. Hackl and R. Heinen, A micromechanical model for pretextured polycrystalline shape–memory alloys including elastic anisotropy, Continuum Mech. Thermodyn. **19**, 499–510 (2008).
[18] K. Hackl and R. Heinen, An upper bound to the free energy of n-variant polycrystalline shape memory alloys, J. Mech. Phys. Sol. **56**, 2832–2843 (2008).
[19] K. Hackl, R. Heinen, W. W. Schmahl, and M. Hasan, Experimental verification of a micromechanical model for polycrystalline shape memory alloys in dependence of martensite orientation distributions, Mat. Sc. Engrg. A **481**, 347–350 (2008).
[20] M. Hasan, W. W. Schmahl, K. Hackl, R. Heinen, J. Frenzel, S. Gollerthan, G. Eggeler, M. Wagner, J. Khalil-Allafi, and A. Baruj, Hard x-ray studies of stress-induced phase transformations of superelastic niti shape memory alloys under uniaxial load, Mat. Sc. Engrg. A **481**, 414–419 (2008).
[21] R. Heinen and K. Hackl, On the calculation of energy-minimizing phase fractions in shape memory alloys, Comp. Meth. Appl. Mech. Engrg. **196**, 2401–2412 (2007).
[22] R. Heinen, U. Hoppe, and K. Hackl, Prediction of microstructural patterns in monocrystalline shape memory alloys using global energy minimization, Mat. Sc. Engrg. A **481**, 362–365 (2008).
[23] D. Helm and P. Haupt, Shape memory behaviour: modelling within continuum mechanics, Int. J. Sol. Struct. **40**, 827–849 (2003).
[24] R. James and K. Hane, Martensitic transformations and shape memory materials, Acta mater. **48**, 197–222 (2000).
[25] R. V. Kohn and S. Mueller, Branching of twins near an austenite–twinned–martensite interface, Phil. Mag. A **66**, 697–715 (1992).
[26] R. V. Kohn and S. Mueller, Surface energy and microstructure in coherent phase transitions, Comm. Pure Appl. Mech. **47**, 405–435 (1994).
[27] R. V. Kohn and G. Strang, Explicit relaxation of a variational problem in optimal design, Bull. Am. Math. Soc. **9**, 211–214 (1983).
[28] R. V. Kohn and G. Strang, Optimal design and relaxation of variational problem i, ii, iii, Comm. Pure Appl. Mech. **39**, 113–137, 139–182, 353–377 (1986).
[29] R. Kohn, The relaxation of a double-well energy, Cont. Mech. Thermodyn. **3**, 193–236 (1991).
[30] M. Kruzik and F. Otto, A phenomenological model for hysteresis in polycrystalline shape memory alloys, Z. Angew. Math. Mech. **84**, 835–842 (2004).
[31] Johnson Matthey Inc., Selected Properties of NiTi, World Wide Web, http://www.jmmedical.com/html/selected_properties.html, 2008.
[32] N. G. Meyers, Quasi–convexity and lower semicontinuity of multiple variational integrals of any order, Trans. Amer. Math. Soc. **119**, 225–249 (1965).
[33] A. Mielke and F. Theil, A mathematical model for rate-independent phase transformations with hysteresis, in: Proceedings of the Workshop on Models of Continuum Mechanics in Analysis and Engineering, edited by R. B. H.-D. Alber and R. Farwig (1999).
[34] A. Mielke, F. Theil, and V. Levitas, A variational formulation of rate-independent phase transformations using an extremum principle, Arch. Rat. Mech. Anal. **162 (2)**, 137–177 (2002).
[35] C. B. Morrey, Quasi–convexity and the lower semicontinuity of multiple integrals, Pacific J. Math. **2**, 25–53 (1952).
[36] M. Ortiz and E. Repetto, Nonconvex energy minimization and dislocation structures in ductile single crystals, J. Mech. Phys. Sol. **47**, 397–462 (1999).
[37] M. Ortiz and L. Stainier, The variational formulation of viscoplastic constitutive updates, Comp. Methods Appl. Mech. Engrg. **171**, 419–444 (1999).
[38] S. Pagano, P. Alart, and O. Maisonneuve, Solid-solid phase transition modelling. local and global minimizations of non-convex and relaxed potentials. isothermal case for shape memory alloys, Int. J. Eng. Sci. **36**, 1143–1172 (1998).
[39] B. Raniecki, C. Lexcellent, and K. Tanaka, Thermodynamic models of pseudoelastic behaviour of shape memory alloys, Arch. Mech. **44**, 261–284 (1992).
[40] M. Schmidt-Baldassari, Numerical concepts for rate-independent single crystal plasticity, Comp. Methods Appl. Mech. Engrg. **192**, 1261–1280 (2003).
[41] P. Sedlak, H. Seiner, M. Landa, V. Novak, P. Sittner, and L. Manosa, Elastic constants of bcc austenite and 2h orthorhombic martensite in cualni shape memory alloy, Acta Materialia **53**, 3643–3661 (2005).
[42] Y. Shu and J. Yen, Multivariant model of martensitic microstructure in thin films, Acta Mater. **56**, 3969–3981 (2008).
[43] M. Šilhavý, The Mechanics and Thermodynamics of Continuous Media (Springer, New York, 1997).
[44] J. C. Simo and T. J. R. Hughes, Computational Inelasticity (Springer, New York, 1998).
[45] V. Smyshlyaev and J. Willis, On the relaxation of a three-well energy, Proc. R. Soc. London A **455**, 779–814 (1998).

 